

Fluorescence Correlation Spectroscopy

Experiment FCS - sjh, rd

University of Florida — Department of Physics
PHY4803L — Advanced Physics Laboratory

Objective

Fluorescence correlation spectroscopy describes a range of techniques that use the fluorescence of diffusing molecules to measure dynamical properties of those molecules, including their rate of diffusion, chemical reaction rates, and more. You will use a basic setup to study the diffusion of fluorescing polymer nanospheres and fluorescing dye molecules to calibrate the apparatus and learn about the technique. Then, you will perform a biological study on the opening and closing of genetically engineered DNA hairpin loops.

References

- R. Rieger, C. Roker, G.U. Nienhaus, *Fluctuation correlation spectroscopy for the advanced physics laboratory*, Am. J. Phys. **73** 1129-1134 (2005).
- D. Magde, E.L. Elson, and W.W. Webb, *Thermodynamic fluctuations in a reacting system: Measurement by fluorescence correlation spectroscopy*, Phys. Rev. Lett., **29** 705-708 (1972)
- E. Haustein and P. Schwille, *Fluorescence correlation spectroscopy: Novel variations of an established technique*, Ann. Rev. Biophys. Biomolec. Struct. **36** 151-169 (2007).
- O. Krichevsky and G. Bonnet, *Fluorescence correlation spectroscopy: the technique and its applications*, Rep. Prog. Phys. **65** 251-297 (2002).
- Ted A. Laurence, Samantha Fore and Thomas Huser, *Fast, flexible algorithm for calculating photon correlations*, Optics Letters **31** 829-831 (2006).
- L.-L. Yang, H.-Y. Lee, M.-K.Wang, X.-Y. Lin, K.-H. Hsu, Y.-R. Chang, W. Fann and J.D. White, *Real-time data acquisition incorporating high-speed software correlator for single-molecule spectroscopy*, J. of Microscopy **234** 302-310 (2009).
- Grégoire Bonnet, Oleg Krichevsky, and Albert Libchaber, *Kinetics of conformational fluctuations in DNA Hairpin-loops*, Proc. Natl. Acad. Sci. USA, **95** 8602-8606, July 1998 Biophysics.

Introduction

There are many situations in biology where it is desirable to characterize biomolecules (e.g. proteins, nucleic acids, etc.) that are present in very small concentrations: How many copies of a particular molecule are present? How quickly does it diffuse through its environment? How does it bind or interact with

other structures or chemical species that are present? Ideally, the experimentalist would be able to make such measurements on the molecules inside a living cell. While it is already difficult to imagine counting the number of copies of a particular chemical species inside a cell, it may seem even harder to believe that important physical and chemical properties (such as diffusion coefficients, reaction equilibria, etc.) of these molecules can also be measured inside the cell in a manner that is non-destructive to both the cell and the chemical species itself. Amazingly, all this can be accomplished through fluorescence correlation spectroscopy (FCS), a technique that was first described by Magde, et al. in the early 1970s and then developed and advanced intensively by a number of physicists during the subsequent decades. FCS is remarkable in part because the technique explicitly assumes and requires that the molecule of interest is present in very small numbers. Its invention was therefore an important early step in the development of the many single-molecule microscopy techniques that have subsequently transformed cell biology since the early 2000's. It is now widely used, with new applications and variations being invented and reported regularly.

The essential idea of FCS is that when a fluorescent molecule, or *fluorophore*, is present at low concentrations in a sample, the fluorescence signal collected from that sample is subject to random fluctuations as the molecules diffuse into and out of the field of view. The fewer the number of molecules present, the larger (in a relative sense) these fluctuations become. The fluorescence collected from a small group of diffusing molecules looks a lot like random noise. However, the faster those molecules diffuse, react, or interact, the faster the fluorescence signal will fluctuate. Therefore, by studying the amplitude and frequency

properties of that noise, we can determine fundamental physical and chemical properties of the system.

In this experiment you will use FCS to measure the concentration and diffusion constant of fluorophores, fluorescent nanospheres, and fluorescently-tagged DNA. The DNA is a so-called “hairpin”, consisting of a single strand of DNA that can bend around itself and form a closed or end-to-end loop; FCS allows you to characterize the rapid opening and closing of this loop simply by observing the fluorescence fluctuations of the DNA.

Apparatus

The experimental configuration for a basic FCS apparatus is fairly simple. A laser beam is brought to a sharp focus within a sample containing a fluorophore and some of the fluorescent light is collected and sent to a photon detector. Figure 1 shows the details for our apparatus.

Two mirrors (not shown in Fig. 1) steer the 532 nm laser beam (green rays in the figure) into the spatial filter. The spatial filter, which smooths the laser beam intensity profile, consists of a focusing lens (L1, fl. = 40 mm), which focuses the laser beam onto a pinhole (P1, $d = 20 \mu\text{m}$) and then a collimating lens (L2, fl. = 60 mm) re-collimates the beam exiting the pinhole.

The beam exiting L2 is steered into the dichroic mirror (M1) using two more mirrors (not shown in Fig. 1). The dichroic mirror reflects about 98% of the 532 nm laser light into the back aperture of a microscope objective (100 \times , oil immersion). The remaining laser light (about 2%) passes through the dichroic mirror and strikes the photodiode. The output current from the photodiode is used to determine the incident laser power on the sample.

The microscope objective focuses the beam

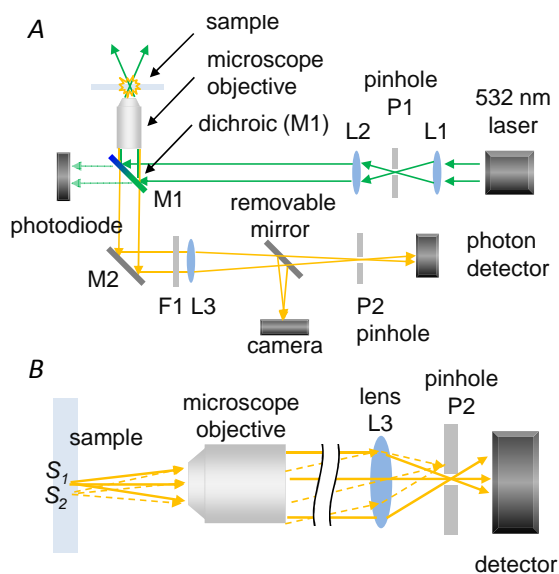


Figure 1: (A) Optical configuration shows the excitation laser (green rays), spatial filter (L1, P1, L2), dichroic mirror (M1), microscope objective, and photodiode. The objective brings the laser to a focus within the sample. Fluorescence emission from the sample (orange rays) is collected by the objective and directed through a laser-blocking filter F1 before it is focused by L3 onto the pinhole P2 and then to the photon detector or, with the removable mirror installed, onto the camera. (B) The pinhole (P2) placed in the image plane allows rays from point S_1 in the sample to reach the detector, but blocks rays arriving from S_2 .

to a diffraction-limited spot within the sample, exciting the fluorescence. Fluorescent emission is at wavelengths longer than the 532 nm laser light (orange lines in the figure) and some of it is collected and collimated by the objective, which directs it back toward the dichroic mirror (M1). The dichroic transmits the longer wavelength light into a mirror (M2) which steers it toward a laser-blocking (long-pass) filter (F1) and a converging lens (L3, fl. = 200 mm). This lens refocuses the light onto the second pinhole (P2, $d = 75 \mu\text{m}$) after which is a photomultiplier tube (PMT) for detecting individual photons getting through

the pinhole.

A removable mirror can be placed in front of P2 to divert the light onto a color CCD camera that can be used for imaging the sample area. These images can be used to determine the magnification and for other diagnostics.

In addition to the fluorescent light from the excitation volume, a fraction of the incident laser light is reflected from the sample (or from the microscope slide holding the sample) and is also collected by the objective. The reflected laser light must be attenuated or it would swamp the smaller intensity of the fluorescence. As it passes back through the dichroic mirror, roughly 98% of the 532 nm laser is reflected back toward the source, while most of the longer-wavelength fluorescent light is transmitted through to the detector. The longpass filter (F1 in Fig. 1) is needed to remove any residual laser light transmitted by the dichroic.

The photon detector module (Hamamatsu, H10682-110) contains a photomultiplier tube (PMT), high voltage power supply, and pulse processing electronics. Inside the PMT a light-sensitive photocathode emits an electron when struck by a visible light photon. The emitted electron is accelerated by a high voltage into a second electrode where 5-10 electrons are ejected and likewise accelerated into a third electrode. Charge multiplication—each time by a factor of 5-10—continues via a cascade of collisions with an additional 10-12 electrodes (dynodes) to produce a burst of 10^6 - 10^8 electrons on the final electrode (anode). For each incident photon, the module converts this anode charge into a single output voltage pulse with an amplitude of 2 V and a width of 20 ns. The frequency or rate of these pulses as a function of time will be denoted $R(t)$ in the theory.

A key principle in FCS experimental design is the need to minimize both the *excitation volume* and the *detection volume* and to get

the best possible overlap between them. The detection volume is the region within the sample from which emitted light can reach the detector. The excitation volume is the region within the sample, centered on the laser focal spot, where the laser intensity is largest. If the detection volume is too large, the PMT will, in effect, detect the spatially-averaged concentration of fluorophores, rather than the locally fluctuating concentration. Fluctuations in the detected light will be minimal and it will not be possible to perform the analysis. If the excitation volume is much larger than the detection volume, diffusing fluorophores will have been in the laser beam for some time before getting into the detection volume. This pre-illumination has several unwanted effects on the excitation-fluorescence process once the fluorophores enter the detection region. If the excitation and detection volume do not overlap well, many of the fluorescence photons will go undetected and the signal will be weak. Therefore, to generate a strong fluctuation signal, the laser excitation should be restricted to the smallest possible volume within the sample, and the detector's field of view must be limited so that only photons from that small volume are detected efficiently.

After excitation by the laser and subsequent fluorescent emission, the fluorophore is ready for another round of excitation-fluorescence. When illuminated with a laser, typical fluorophores fluoresce at rates of 10 kHz or more. However, the excitation can sometimes temporarily “shelve” the fluorophore in a long-lived electronic triplet-state which will not fluoresce again until the triplet state decays. In addition, fluorophores in excited electronic states can chemically interact with other fluorophores or surrounding molecules and become destroyed—permanently unable to participate in the excitation-fluorescence process. These “burned out” fluorophores are said to

be *photobleached*. A photobleached sample will not fluoresce. The longer the exposure to the laser light and the higher the laser intensity, the more likely the fluorophore is to end up shelved or photobleached. Since both processes lead to an average fluorescence that is weaker than normal, it will also be important to use a laser power that is not any larger than necessary to obtain a strong fluorescent signal.

The beam exiting directly from the laser has a somewhat irregular intensity profile and therefore—if focused by the microscope objective—will not focus to a sharp, diffraction-limited spot. Inserting a spatial filter (L1, P1, L2 in Fig. 1A) smooths the intensity profile and consequently reduces the spot size. One may think of the optical system as using intense laser light to illuminate the pinhole aperture, and then projecting a sharp, real image of that illuminated aperture onto the sample.

We define a geometry where the microscope slide is oriented parallel to the xy plane (see Fig. 2), the laser beam propagates in the $+z$ direction, and the center of the beam focus is $\mathbf{r} = 0$. In the focal plane at $z = 0$, the laser intensity pattern is reasonably well-described by a Gaussian:

$$I(x, y, z = 0) = I_0 \exp\left(-2\frac{x^2 + y^2}{w_0^2}\right) \quad (1)$$

where

$$I_0 = \frac{2P}{\pi w_0^2} \quad (2)$$

and P is the total laser power exiting the objective. I_0 is the maximum intensity at the center of the laser spot and w_0 describes the radius of the spot in the horizontal plane. The prefactor of 2 in the argument of the exponential is traditional in laser optics formulas and implies that the intensity a distance w_0 from the origin has dropped off by a factor of e^{-2} ,

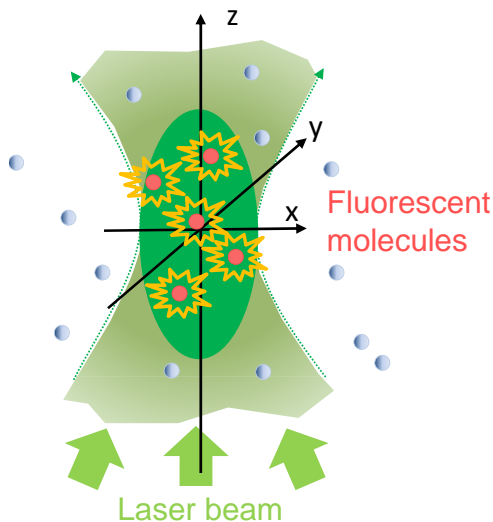


Figure 2: Laser light is brought to a focus on a solution containing a low concentration of fluorescent molecules. The molecules emit light as they diffuse through the intense focal region and are excited by the laser beam.

i.e., to 14% of its maximum, and 86% of the beam power is inside this radius.

The smallest possible (diffraction limited) spot size has a radius $w_0 \approx \lambda/2 \text{N.A.}$ where the numerical aperture for our objective $\text{N.A.} = 1.4$ gives a value for w_0 around $0.2 \mu\text{m}$. Our apparatus typically gives $w_0 \approx 0.3 \mu\text{m}$ —a bit larger than the diffraction limit.

The laser beam is sharply focused by the objective and converges quickly coming into the laser spot and diverges quickly coming out. Consequently, its intensity also decreases away from $z = 0$ and can be well modeled as follows

$$I(x, y, z) = I_0(z) \exp\left(-2\frac{x^2 + y^2}{w(z)^2}\right) \quad (3)$$

where the on-axis intensity $I_0(z)$ falls off as

$$I_0(z) = \frac{I_0}{1 + (z/z_0)^2} \quad (4)$$

and the spot size increases as

$$w^2(z) = w_0^2 \left(1 + (z/z_0)^2\right) \quad (5)$$

z_0 describes the length scale in the z -direction for the fall-off in laser intensity. It is related to w_0 by

$$z_0 = \frac{\pi w_0^2}{\lambda} \quad (6)$$

and is a few times larger than w_0 .

The pinhole scheme is used again to ensure that only light from the excitation volume reaches the photon detector. The microscope objective and lens L3 together form a microscope that projects a magnified, real image of the illuminated sample onto the image plane. This is a so-called *confocal* configuration (see Fig. 1B); a pinhole in the image plane allows only the light within one small area of the image to reach the detector. Of course, that light originates from the corresponding region of the sample, and thus the pinhole prevents the detector from “seeing” other regions of the sample. This detection area at the sample is a reduced or demagnified real image of the pinhole P2. Our apparatus uses a pinhole diameter of $75 \mu\text{m}$ and has a magnification of about 100. Thus, the pinhole only allows light from about a $0.75 \mu\text{m}$ diameter circular detection area at the sample to pass through to the photon detector. The P2 pinhole size is specifically chosen so that the diameter of the detection area matches the $2w_0$ diameter of the focused laser spot reasonably well. Note that the detection pinhole must be precisely positioned in the xy direction if it is to overlap with the bright fluorescence emission spot that is being produced by the microscope objective in the image plane; the pinhole is mounted on an xy micrometer stage in order to facilitate this positioning.

The optics/pinhole also affect the collection efficiency for fluorescent emissions from fluorophores away from $z = 0$. Fluorescent pho-

tons are emitted in all directions and even at $z = 0$, only a fraction of those photons emitted toward the objective will be collected by it and sent on to the image plane. The fraction collected is proportional to the solid angle collected by the objective. This solid angle is largest at $z = 0$, where it depends on objective design, specifically its numerical aperture or NA. The solid angle collected, and thus the collection efficiency, falls off rapidly away from $z = 0$. This is because away from $z = 0$, only those photons that appear—were their path extended forward or backward—as if they could have come from the $0.75\ \mu\text{m}$ detection area will be collected by the objective and make it through the pinhole. In this way, the optics/pinhole define a detection volume and efficiency that depends on x , y and z .

The volume common to both the excitation volume and the detection volume will be called the *measurement volume*. Let $dR(t)$ represent the rate (photons/s) at which fluorescence photons arrive at the detector from a very small volume element dV located at a position \mathbf{r} within the measurement volume. $dR(t)$ is determined by the product of the concentration $C(\mathbf{r}, t)$ of the fluorophore, the laser beam intensity $I(\mathbf{r})$, the efficiency with which the fluorophore converts laser excitation energy to fluorescent emission, and the detection efficiency with which emitted photons are turned into pulses by the PMT module. It will be convenient to define an overall efficiency $\Phi(\mathbf{r})$ that accounts for all factors except for the fluorophore concentration. That is, we can write

$$dR(t) = \Phi(\mathbf{r})C(\mathbf{r}, t)dV \quad (7)$$

Equation 7 assumes that the fluorophore emits fluorescent photons at a rate proportional to the laser intensity at that point and nothing else. For example, it does not account for photobleaching, shelving, or any other mechanisms by which the fluorophore

efficiency changes in time or with laser intensity. Taking such mechanisms into effect when making predictions is non-trivial and so this assumption should be checked by taking data at several laser powers.

If the P2 pinhole is properly positioned so that the detection volume overlaps the excitation volume, $\Phi(\mathbf{r})$ can be approximated by a three dimensional measurement Gaussian

$$\Phi(\mathbf{r}) = \Phi_0 \exp\left(-2\frac{x^2 + y^2}{w_{xy}^2} - 2\frac{z^2}{w_z^2}\right) \quad (8)$$

where w_{xy} is roughly equal to the laser beam spot radius (w_0 in Eq. 1) and w_z (roughly z_0 in Eq. 4 and 5) is a few times larger.

Where the argument in parentheses above is equal to one

$$\frac{x^2 + y^2}{w_{xy}^2} + \frac{z^2}{w_z^2} = 1 \quad (9)$$

describes an ellipsoid with a circular cross section of radius w_{xy} in the x - and y -directions and a radius w_z in the z -direction. On this ellipse, the efficiency has fallen to about 14% of its maximum. The volume inside this ellipse is $4\pi\omega w_{xy}^2 w_z/3$. Taking reasonable estimates: $w_{xy} = 0.4\ \mu\text{m}$ and $w_z = 3\ \mu\text{m}$, fluorescence is detected as individual particles diffuse through a measurement volume $V \approx 1\ \mu\text{m}^3 \approx 10^{-15}\ \text{l}$ or around 1 femtoliter.

To find the overall rate from the sample, Eq. 7 must be integrated over all volume elements.

$$R(t) = \int d^3r \Phi(\mathbf{r})C(\mathbf{r}, t) \quad (10)$$

where we have used a shorthand notation for triple integrations

$$\int d^3r = \int_{-\infty}^{\infty} \int_{-\infty}^{\infty} \int_{-\infty}^{\infty} dx dy dz \quad (11)$$

Theory

FCS can be used to study experimental samples that contain multiple species of fluorescent molecules with different concentrations C_i and diffusion coefficients D_i (where $i = 1, 2, \dots, N_{\text{species}}$). Here, we develop the theory of FCS for the simpler case in which the sample contains a single fluorescent species with concentration C and diffusion coefficient D . For multiple diffusing species the mathematics are more complex but not fundamentally different. In the following we present a simplified ($N_{\text{species}} = 1$) version of the multiple-species theory as presented by Krichevsky and Bonnet.

In a well-mixed solution at chemical and thermal equilibrium, the concentration of the fluorescent species will have a uniform steady-state value \bar{C} , where this value represents an average over macroscopic scales of time and distance. Over microscopic scales, however, the particles are in continuous motion (diffusive, i.e., Brownian motion) and so when averaged over these much smaller length scales, the concentration $C(\mathbf{r}, t)$ tends to fluctuate in space and time. (See Figure 3.) The smaller the averaging volume, the larger the fluctuations.

Fluctuations in the concentration are created continuously by random Brownian forces while they simultaneously decay over time according to the diffusion equation

$$\frac{\partial C(\mathbf{r}, t)}{\partial t} = D\nabla^2 C(\mathbf{r}, t) \quad (12)$$

where D is the diffusion coefficient of the fluorescent molecules.

Note that we can also write $C(\mathbf{r}, t)$ as the sum of its constant average \bar{C} and its time- and space-dependent fluctuation $\delta C(\mathbf{r}, t)$:

$$C(\mathbf{r}, t) = \bar{C} + \delta C(\mathbf{r}, t) \quad (13)$$

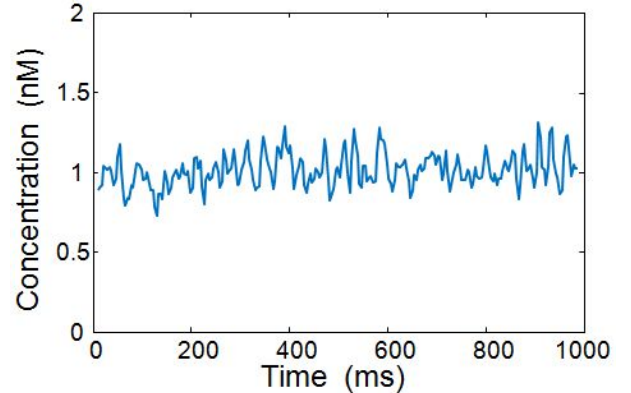


Figure 3: While the average concentration—here, $\bar{C} \simeq 1$ nM—remains constant, the instantaneous concentration of fluorescent molecules $C(\mathbf{r}, t)$ averaged over a finite (but small) volume fluctuates with time as the molecules diffuse in and out of that volume.

With this definition, the temporal and spatial averages of $\delta C(\mathbf{r}, t)$ will both be zero. Moreover, because \bar{C} is constant, using Eq. 13 in the diffusion equation 12 gives

$$\frac{\partial \delta C(\mathbf{r}, t)}{\partial t} = D\nabla^2 \delta C(\mathbf{r}, t) \quad (14)$$

Equation 14 describes a simple relationship between the temporal and spatial behavior of the fluctuations $\delta C(\mathbf{r}, t)$. At locations where C is a maximum, i.e., where the second spatial derivative of δC is negative, the time derivative of δC is negative, and so δC must decrease in time. Further, the sharper the maximum in δC , the more rapidly these local maxima dissipate. Conversely, where the second derivative is positive so that δC is locally at a minimum, the concentration must increase over time; local “gaps” in concentration tend to fill in over time. In this way, Eq. 12 (or Eq. 14) state that fluctuations or inhomogeneities in the concentration tend to smooth themselves out, and that the rate of smoothing is faster where δC has a steeper gradient.

As we will see, the most useful information

is contained in the *relative* changes in the fluorescence $R(t)$ collected from an excited volume. The problem is to figure out how to extract that information: $R(t)$ fluctuates continuously as individual particles diffuse through the measurement volume. Because these fluctuations are random in time, there is not much gained from studying $R(t)$ directly. It is more useful to examine statistical properties of $R(t)$ associated with its fluctuations as these can be related to important physical parameters (D , \bar{C} , w_{xy} , w_z , etc.) of the experiment.

Autocorrelation

As we are interested in fluctuations of $R(t)$, we will focus on the quantity

$$\delta R(t) = R(t) - \bar{R} \quad (15)$$

using this with Eqs. 10 and 13, defines \bar{R} as the temporal average of $R(t)$

$$\bar{R} = \int d^3r \bar{C} \Phi(\mathbf{r}) \quad (16)$$

and $\delta R(t)$ as due to the fluctuations in $C(\mathbf{r}, t)$

$$\delta R(t) = \int d^3r \Phi(\mathbf{r}) \delta C(\mathbf{r}, t) \quad (17)$$

$\delta R(t)$ changes randomly over time and we anticipate that it will change more rapidly if the particles diffuse more rapidly, or if the detection volume is smaller. Therefore, we wish to characterize the time dependence of $\delta R(t)$ in a statistical way. A good way to do this is to study the *autocorrelation* of $\delta R(t)$, defined as

$$G(t) = \frac{\langle \delta R(t') \delta R(t' + t) \rangle}{\bar{R}^2} \quad (18)$$

The angle brackets in the numerator indicate an ensemble average, meaning an average over many (hypothetical) implementations of the

system and the measurement. The autocorrelation compares δR at a time t' with its value at a later time $t' + t$ (see Fig. 4). Suppose that δR requires a time τ to change significantly. Consequently, for $t < \tau$, $\delta R(t' + t)$ is likely to have the same sign as $\delta R(t')$; the product $\delta R(t) \delta R(t' + t)$ will usually be positive, thereby leading to $G(t) > 0$. However, for $t \gg \tau$ we expect that δR will have changed considerably between t' and $t' + t$; $\delta R(t' + t)$ will be equally likely to be positive or negative no matter what sign $\delta R(t')$ had; the product $\delta R(t') \delta R(t' + t)$ will be equally likely to be positive or negative and it will average to zero. Consequently, $G(t)$ will approach zero as $t \rightarrow \infty$.

We will assume that the fluctuations are stationary, in the sense that the statistics of δR will be no different if we study them now than if we study them later this afternoon. (Assume that the sample doesn't dry out!) In that case, the time t' in Eq. 18 might as well be $t' = 0$ and we can rewrite Eq. 18 as

$$G(t) = \frac{\langle \delta R(0) \delta R(t) \rangle}{\bar{R}^2} \quad (19)$$

where the angle brackets should be interpreted as an expectation value, i.e., as an average over infinitely many samples of the product of δR at some point in time and its value a time t later.

Using Eq. 17 in Eq. 19 tells us that, in order to relate $G(t)$ to the physical parameters D , \bar{C} , etc., we need to evaluate

$$G(t) = \frac{1}{\bar{R}^2} \int d^3r \int d^3r' \Phi(\mathbf{r}) \Phi(\mathbf{r}') \langle \delta C(\mathbf{r}, 0) \delta C(\mathbf{r}', t) \rangle \quad (20)$$

where the expectation value brackets have been moved inside the d^3r and d^3r' integrals where they are applied only to the product of the concentrations as the concentration is the

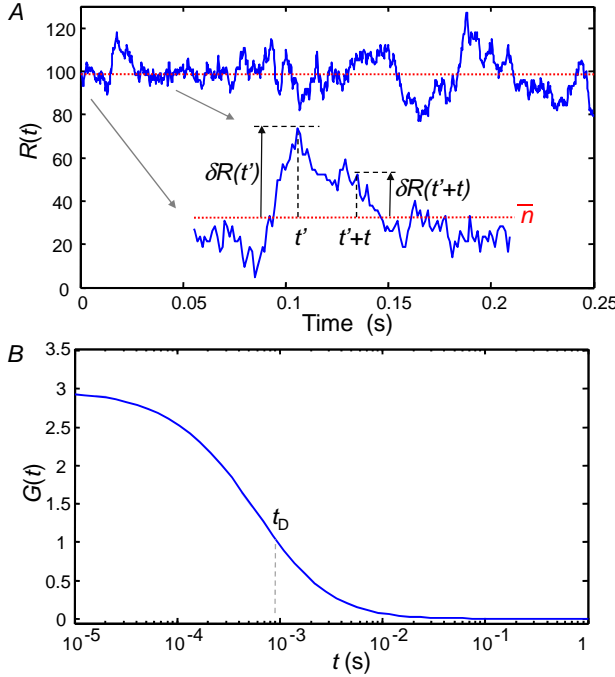


Figure 4: (A) The photon count rate $R(t)$ fluctuates randomly around its average value \bar{R} . *Inset:* The autocorrelation function $G(t)$ characterizes the average similarity between $\delta R(t')$ and $\delta R(t'+t)$. For shorter intervals t , both δR are likely to be of the same sign, leading to a positive $G(t)$. For longer intervals t , the fluctuations are uncorrelated and $G(t) \rightarrow 0$. (B) The calculated autocorrelation function (Eq. 54) is shown for $t_D = 0.9$ ms, $\omega = 1$ and $\bar{N} = 0.34$.

only quantity that fluctuates randomly. The trick will be to calculate this expectation value using the diffusion equation for $\delta C(\mathbf{r}, t)$ and a property of $\delta C(\mathbf{r}, t)$ related to Poisson statistics.

We start by defining the Fourier transform (in all three dimensions) of $\delta C(\mathbf{r}, t)$.

$$\tilde{C}(\mathbf{q}, t) = \frac{1}{(2\pi)^{3/2}} \int d^3r \delta C(\mathbf{r}, t) e^{i\mathbf{q}\cdot\mathbf{r}} \quad (21)$$

for which the inverse transform is

$$\delta C(\mathbf{r}, t) = \frac{1}{(2\pi)^{3/2}} \int d^3q \tilde{C}(\mathbf{q}, t) e^{-i\mathbf{q}\cdot\mathbf{r}} \quad (22)$$

where $\mathbf{q}\cdot\mathbf{r} = q_x x + q_y y + q_z z$ and the shorthand notation is again used for the triple integration in \mathbf{q} ($d^3q = dq_x dq_y dq_z$, with integration limits from $-\infty$ to ∞). Inserting Eq. 22 into the diffusion equation, Eq. 14, noting that $\nabla^2 e^{-i\mathbf{q}\cdot\mathbf{r}} = -q^2 e^{-i\mathbf{q}\cdot\mathbf{r}}$ (where, of course, $q^2 = \mathbf{q}\cdot\mathbf{q} = q_x^2 + q_y^2 + q_z^2$) gives

$$\int d^3q e^{-i\mathbf{q}\cdot\mathbf{r}} \left(\frac{\partial \tilde{C}(\mathbf{q}, t)}{\partial t} + Dq^2 \tilde{C}(\mathbf{q}, t) \right) = 0 \quad (23)$$

For this equation to be true, the term in parentheses must be zero for all q and solving it gives

$$\tilde{C}(\mathbf{q}, t) = \tilde{C}(\mathbf{q}, 0) e^{-Dq^2 t} \quad (24)$$

where, in order to satisfy initial conditions, $\tilde{C}(\mathbf{q}, 0)$ must be the Fourier transform of $\delta C(\mathbf{r}, 0)$

$$\tilde{C}(\mathbf{q}, 0) = \frac{1}{(2\pi)^{3/2}} \int d^3r \delta C(\mathbf{r}, 0) e^{i\mathbf{q}\cdot\mathbf{r}} \quad (25)$$

For the Fourier transform at least, we have found the time dependence of δC .

Now rewrite the expectation value using Eq. 22 and then Eq. 24

$$\begin{aligned} \langle \delta C(\mathbf{r}, 0) \delta C(\mathbf{r}', t) \rangle &= \frac{1}{(2\pi)^{3/2}} \left\langle \delta C(\mathbf{r}, 0) \int d^3q e^{-i\mathbf{q}\cdot\mathbf{r}'} \tilde{C}(\mathbf{q}, t) \right\rangle \\ &= \frac{1}{(2\pi)^{3/2}} \int d^3q e^{-i\mathbf{q}\cdot\mathbf{r}'} e^{-Dq^2 t} \langle \delta C(\mathbf{r}, 0) \tilde{C}(\mathbf{q}, 0) \rangle \end{aligned} \quad (26)$$

Using Eq. 25 to substitute for $\tilde{C}(\mathbf{q}, 0)$ (using the dummy integration variable \mathbf{r}'' as \mathbf{r} and \mathbf{r}' are already in use) then gives

$$\begin{aligned} \langle \delta C(\mathbf{r}, 0) \delta C(\mathbf{r}', t) \rangle &= \frac{1}{(2\pi)^3} \int d^3q e^{-i\mathbf{q}\cdot\mathbf{r}'} e^{-Dq^2 t} \int d^3r'' e^{i\mathbf{q}\cdot\mathbf{r}''} \\ &\quad \langle \delta C(\mathbf{r}, 0) \delta C(\mathbf{r}'', 0) \rangle \end{aligned} \quad (27)$$

As discussed in more detail below, the bracketed expression in the above integral is proportional to a delta function $\delta(\mathbf{r} - \mathbf{r}'')$. Together with the Poisson statistics of fluctuations in the number of particles in any given volume, this means that the final integral in this equation satisfies

$$\int d^3 r'' e^{i\mathbf{q}\cdot\mathbf{r}''} \langle \delta C(\mathbf{r}, 0) \delta C(\mathbf{r}'', 0) \rangle = \bar{C} e^{i\mathbf{q}\cdot\mathbf{r}} \quad (28)$$

So that Eq. 27 becomes

$$\begin{aligned} & \langle \delta C(\mathbf{r}, 0) \delta C(\mathbf{r}', t) \rangle \\ &= \frac{\bar{C}}{(2\pi)^3} \int d^3 q e^{-Dq^2 t} e^{-i\mathbf{q}\cdot\mathbf{r}'} e^{i\mathbf{q}\cdot\mathbf{r}} \end{aligned} \quad (29)$$

Along with the diffusion equation, the transformation from Eq. 27 to Eq. 29 is at the heart of the theory and worth deriving.

More generally one can show

$$\int d^3 r'' \langle \delta C(\mathbf{r}, 0) \delta C(\mathbf{r}'', 0) \rangle f(\mathbf{r}'') = \bar{C} f(\mathbf{r}) \quad (30)$$

where $f(\mathbf{r}'')$ is an arbitrary function of \mathbf{r}'' . Equation 30 is equivalent to the substitution

$$\langle \delta C(\mathbf{r}, 0) \delta C(\mathbf{r}'', 0) \rangle = \bar{C} \delta(\mathbf{r} - \mathbf{r}'') \quad (31)$$

where $\delta(\mathbf{r} - \mathbf{r}'')$ is the Dirac delta function satisfying

$$\int d^3 r'' f(\mathbf{r}'') \delta(\mathbf{r} - \mathbf{r}'') = f(\mathbf{r}) \quad (32)$$

To see how Eq. 30 comes about it is useful to consider the integration over $d^3 r''$ as being performed numerically on an equally-spaced three dimensional Cartesian grid. Let the grid spacing be ℓ in all three directions so that the volume elements will all have a volume $\Delta V = \ell^3$. Each grid cell is centered on one position $\mathbf{r}'' = \mathbf{r}_j$ in the grid so that the left side integral of Eq. 30 for one particular $\mathbf{r} = \mathbf{r}_i$ becomes:

$$\begin{aligned} & \int d^3 r'' \langle \delta C(\mathbf{r}_i, 0) \delta C(\mathbf{r}'', 0) \rangle f(\mathbf{r}'') \\ &= \sum_{\text{all } j} \Delta V \langle \delta C(\mathbf{r}_i, 0) \delta C(\mathbf{r}_j, 0) \rangle f(\mathbf{r}_j) \end{aligned} \quad (33)$$

where the sum is over grid points covering all space.

Without loss of generality, we will choose $\mathbf{r} = \mathbf{r}_i$ as located exactly at the center of one particular cell in the sum over j . That is, exactly one of the \mathbf{r}_j in the sum will be located at \mathbf{r}_i . Moreover, the \mathbf{r}_i will also be associated with a cell, again of volume $\Delta V = \ell^3$, which, for $j = i$, will then be the exact same cell as the one centered around \mathbf{r}_j . For all other j , the cells will not have any common volume.

Now bring two ΔV 's into the expectation value on the right side of Eq. 33 transforming it to

$$S = \frac{1}{\Delta V} \sum_{\text{all } j} \langle \Delta V \delta C(\mathbf{r}_i, 0) \Delta V \delta C(\mathbf{r}_j, 0) \rangle f(\mathbf{r}_j) \quad (34)$$

Each factor in the expectation value is now the product of a concentration fluctuation $\delta C(\mathbf{r}, 0) = C(\mathbf{r}, 0) - \bar{C}$ multiplied by a volume $\Delta V = \ell^3$. Of course,

$$\bar{n} = \Delta V \bar{C} \quad (35)$$

is just the average concentration times the volume and thus is equal to the average number of fluorophores that can be expected in any cell, while

$$n(\mathbf{r}, 0) = \Delta V C(\mathbf{r}, 0) \quad (36)$$

is the actual number in the cell. Thus, the deviation $\delta n(\mathbf{r}, 0)$ of the number of particles in the cell from the average becomes

$$\begin{aligned} \delta n(\mathbf{r}, 0) &= n(\mathbf{r}, 0) - \bar{n} \\ &= \Delta V (C(\mathbf{r}, 0) - \bar{C}) \\ &= \Delta V \delta C(\mathbf{r}, 0) \end{aligned} \quad (37)$$

Making this substitution, the right side of Eq. 33 becomes

$$S = \frac{1}{\Delta V} \sum_{\text{all } j} \langle \delta n(\mathbf{r}_i, 0) \delta n(\mathbf{r}_j, 0) \rangle f(\mathbf{r}_j) \quad (38)$$

As the fluorophores diffuse under the action of Brownian forces, their number in each cell will change. At any particular time, the number $n(\mathbf{r}, 0)$ in any cell is a random variable. Since all fluorophores follow independent random paths, the probability per unit volume of finding a fluorophore is everywhere constant (and equal to \bar{C}). Consequently, $n(\mathbf{r}, 0)$ must follow a Poisson distribution (with a mean of \bar{n}). If the number in a particular cell is noted at different times and averaged over very long times one should find the average satisfies $\langle n(\mathbf{r}, 0) \rangle = \bar{n}$, i.e.,

$$\langle \delta n(\mathbf{r}, 0) \rangle = 0 \quad (39)$$

and, as is well known for the Poisson distribution, the numbers in any one cell should have a variance (mean of the squared deviation from the mean) $\langle (n(\mathbf{r}, 0) - \bar{n})^2 \rangle$ equal to the average \bar{n} . That is, for any \mathbf{r}

$$\langle (\delta n(\mathbf{r}, 0))^2 \rangle = \bar{n} \quad (40)$$

Moreover, the actual number in different cells will be uncorrelated—the variations in one cell will not depend on the variations of any other cell. At different times the deviations $\delta n(\mathbf{r}, 0)$ will sometimes be positive and sometimes negative. While the square of the deviations in the same cell is always positive and has an average given by Eq. 40, the product of the deviations in different cells will be equally likely to be positive as negative and will average to zero. That is for $j \neq i$,

$$\langle \delta n(\mathbf{r}_i, 0) \delta n(\mathbf{r}_j, 0) \rangle = 0 \quad (41)$$

So now with Eqs. 40 and 41, the sum in Eq. 38 can be performed. The only non-zero term in the sum is for $j = i$ and gives

$$\begin{aligned} S &= \frac{1}{\Delta V} \bar{n} f(\mathbf{r}_i) \\ &= \bar{C} f(\mathbf{r}_i) \end{aligned} \quad (42)$$

Using this in Eq. 33 then gives Eq. 30, thereby proving Eq. 28 and 29.

Now substitute Eq. 29 into Eq. 20 and integrate over \mathbf{r} and \mathbf{r}' to get

$$G(t) = \frac{\bar{C}}{\bar{R}^2} \int d^3 q \tilde{\Phi}(\mathbf{q}) \tilde{\Phi}(-\mathbf{q}) e^{-Dq^2 t} \quad (43)$$

where $\tilde{\Phi}(\mathbf{q})$ is the Fourier transform of $\Phi(\mathbf{r})$:

$$\tilde{\Phi}(\mathbf{q}) = \frac{1}{(2\pi)^{3/2}} \int d^3 r \Phi(\mathbf{r}) e^{i\mathbf{q}\cdot\mathbf{r}} \quad (44)$$

Because $\Phi(\mathbf{r})$ is real, the two Fourier transforms $\tilde{\Phi}(\mathbf{q})$ and $\tilde{\Phi}(-\mathbf{q})$ are complex conjugates and so their product is $|\tilde{\Phi}(\mathbf{q})|^2$. Note that the average photon count rate \bar{R} in the denominator of 43 is

$$\bar{R} = \int d^3 r \Phi(\mathbf{r}) \bar{C} \quad (45)$$

which we can write as

$$\bar{R} = \bar{C} (2\pi)^{3/2} \tilde{\Phi}(0) \quad (46)$$

because the $\mathbf{q} = 0$ Fourier transform component of $\Phi(\mathbf{r})$ is given by

$$\tilde{\Phi}(0) = \frac{1}{(2\pi)^{3/2}} \int d^3 r \Phi(\mathbf{r}) \quad (47)$$

Using this in Eq. 43, $G(t)$ can be expressed in terms of physical parameters such as D and \bar{C} as well as the Fourier transform of the measurement volume $\Phi(\mathbf{r})$:

$$G(t) = \frac{1}{(2\pi)^3 \bar{C} \tilde{\Phi}^2(0)} \int d^3 q |\tilde{\Phi}(\mathbf{q})|^2 e^{-Dq^2 t} \quad (48)$$

Equation 48 may still seem obscure because it contains $\tilde{\Phi}(\mathbf{q})$. However, the Fourier transform of the Gaussian $\Phi(\mathbf{r})$ of Eq. 8 is not difficult to evaluate and gives

$$\tilde{\Phi}(\mathbf{q}) = \frac{\Phi_0 w_{xy}^2 w_z}{8} \exp\left(-\frac{w_{xy}^2 (q_x^2 + q_y^2)}{8} - \frac{w_z^2 q_z^2}{8}\right) \quad (49)$$

Using this in Eq. 48 (not only in the integrand, but also in the scale factor out front $\tilde{\Phi}(0) = \Phi_0 w_{xy}^2 w_z / 8$) leads to

$$G(t) = \frac{1}{(2\pi)^3 \bar{C}} \int d^3q \quad (50)$$

$$\exp\left(-\frac{w_{xy}^2(q_x^2 + q_y^2)}{4} - \frac{w_z^2 q_z^2}{4} - Dq^2 t\right)$$

These Gaussian integrals are also relatively simple to evaluate leading to

$$G(t) = \frac{1}{\pi^{3/2} w_{xy}^2 w_z \bar{C}} \quad (51)$$

$$\left(1 + \frac{t}{t_D}\right)^{-1} \left(1 + \frac{t}{\omega^2 t_D}\right)^{-1/2}$$

In this equation we have defined a diffusion time scale

$$t_D = \frac{w_{xy}^2}{4D} \quad (52)$$

and a dimensionless ratio

$$\omega = \frac{w_z}{w_{xy}} \quad (53)$$

that describes the shape of the focal region. We can think of t_D as (roughly) the time that it takes a molecule to diffuse across the xy dimension of the measurement volume. We can think of the denominator of the prefactor as an effective measurement volume $V_e = \pi^{3/2} w_{xy}^2 w_z$ (about 1/3 larger than the ellipsoid volume of $(4/3)\pi w_{xy}^2 w_z$) multiplied by the average particle concentration \bar{C} , i.e., it is the average number of particles $\bar{N} = \bar{C} V_e$ within the effective measurement volume. This leads to a remarkably simple expression for the autocorrelation function:

$$G(t) = \frac{1}{\bar{N}} \left(1 + \frac{t}{t_D}\right)^{-1} \left(1 + \frac{t}{\omega^2 t_D}\right)^{-1/2} \quad (54) \quad \text{and}$$

The simplicity of this result, after all the work that went into deriving it, is one of the marvels of FCS. Note first that it describes a simple power law behavior. For a single diffusing species, there is a single important time

scale t_D . On time scales much shorter than t_D , $G(t) \rightarrow 1/\bar{N}$ as $t \rightarrow 0$. On much longer time scales, $G(t)$ falls off in power law fashion $G(t) \propto t^{-3/2}$ as $t \rightarrow \infty$. Second, it is noteworthy that $G(t)$ scales inversely with \bar{N} , the average number of particles in the measurement volume: The smaller the number of particles in the sample, the larger the fluctuations and consequently the larger the signal of interest! This seems paradoxical, but it does show why FCS is ideally suited for experiments using very low fluorophore concentrations (e.g., scarce biomolecules) and very small detection volumes (e.g., inside living cells). Of course, when the number of particles becomes exceedingly small, the amount of fluorescent light detected will decrease and can drop below the amount needed to distinguish the fluorescent signal from background due to detector dark counts and counts from non-fluorescent light leaking into the detector.

Exercise 1 Fill in the two missing steps for determining $G(t)$ by deriving Eqs. 49 (from Eq. 44 with Eq. 8) and by deriving Eq. 51 (from Eq. 50). In each case, first show how the triple integral is simply a product of three, one-dimensional integrals of similar form. Determine the one-dimensional integrals and then show how they give the final three-dimensional result. You can use the following two Gaussian integral formulas

$$\int_{-\infty}^{\infty} \exp(-ax^2) dx = \sqrt{\frac{\pi}{a}} \quad (55)$$

and

$$\int_{-\infty}^{\infty} \exp(-ax^2) \cos(bx) dx = \sqrt{\frac{\pi}{a}} \exp\left(-\frac{b^2}{4a}\right) \quad (56)$$

where $a > 0$, but should derive all other results.

More complicated situations

We have considered only the simple case where one fluorescent chemical species is present, characterized by a single diffusion coefficient D . More complex scenarios can also be studied. In the case where the sample contains two fluorescent species that diffuse independently, the signal is additive:

$$\delta R(t) = \delta R_A(t) + \delta R_B(t) \quad (57)$$

As long as $R_A(t)$ and $R_B(t)$ are uncorrelated, the correlation function for $\delta R(t)$ is readily calculated to be the additive sum of the two correlation functions (see Equation 21 of Krichevsky, 2002).

An interesting case occurs when the sample contains two chemical species A and B that interconvert through some form of reaction dynamics:



If only one of these (A say) is actually fluorescent, then the molecular fluorescence blinks on and off depending on the state the molecule is in and the autocorrelation function becomes modified. If the diffusion constants are the same for both species (see Krichevsky (2002)), the diffusion dynamics and the reaction dynamics are independent, and the resulting autocorrelation function becomes a product of the purely diffusive term already derived and an extra factor describing the reaction dynamics.

$$G(t) = \frac{1}{\bar{N}} \left(1 + \frac{t}{t_D}\right)^{-1} \left(1 + \frac{t}{\omega^2 t_D}\right)^{-1/2} (1 + K \exp(-t/\tau)) \quad (59)$$

The reaction dynamics factor $1 + K e^{-t/\tau}$ depends only on the reaction rates in each direction: k_{AB} for $A \rightarrow B$ and k_{BA} for $B \rightarrow A$.

The time constant τ is the relaxation time for the chemical reaction and given by

$$\tau = (k_{AB} + k_{BA})^{-1} \quad (60)$$

and the ratio

$$K = \frac{k_{AB}}{k_{BA}} \quad (61)$$

gives the equilibrium populations of state B to state A

$$K = \frac{\bar{C}_B}{\bar{C}_A} \quad (62)$$

and

$$\bar{N} = (\bar{C}_A + \bar{C}_B)V_e \quad (63)$$

is the average total number of molecules in the effective volume.

For this reason, it is possible to use FCS to measure not only the diffusion coefficient of a chemical species but also the rates and equilibrium constants for its reactions with other species in the environment.

Exercise 2 (a) Show that for $t \ll \tau$ and $t \ll t_D$, $G(t \rightarrow 0) = 1/\bar{N}_A$, i.e., it depends only on the average number of fluorescing molecules \bar{N}_A . (b) Consider the case where $\tau \ll t_D$, i.e., when the molecule switches back and forth between the fluorescing and non-fluorescing states at a rate much faster than the diffusion time through the measurement volume. For this case, show that for $t \gg \tau$, $G(t)$ is the same as a purely diffusive $G(t)$ with an amplitude that depends on the average total number of molecules in the volume, that is, including both the fluorescing and non-fluorescing types. Explain why fast reaction dynamics would be expected to have no effect on $G(t)$ for $t \gg \tau$. Hint: When the molecule diffuses into the measurement volume, the fast reaction dynamics mean it will blink on and off many times before diffusing out of that volume.

Hardware

The Laser

The DPSS (diode-pumped solid state) laser (Thorlabs, DJ532-40) produces a 532 nm beam with an adjustable power up to a maximum of around 40 mW. It starts from a 808 nm diode laser which pumps a Nd:YVO₄ (yttrium orthovanadate) crystal which then lases at 1064 nm. This laser beam is incident on a KTP (potassium titanyl phosphate) crystal which frequency-doubles the laser light to the 532 nm laser beam used in this experiment.

The doubling process is very temperature sensitive and so the laser is housed in a temperature controlled mounting block (Thorlabs, TCLD09) containing laser connections, a 10 k Ω thermistor mounted near the laser, and a Peltier thermoelectric device located between the laser at the front and a heat sink on the back. Two electronics modules are used with the laser/mounting block—a temperature controller and a current controller (Wavelength Electronics, LFI 3500 and LFI 4500, respectively).

When the temperature controller is enabled—by pressing the button to the left of the main temperature adjust knob at the top right of the unit, a current is supplied to the Peltier device in the mounting block. Depending on the direction of the current, the device can heat or cool the laser. The thermistor resistance increases as its temperature decreases and vice versa. The temperature controller puts a fixed 100 μ A current through the thermistor and a feedback circuit compares the resulting thermistor voltage with that requested by the user. A feedback loop in the controller adjusts the Peltier current to keep them equal. The temperature adjust knob is used with the main LED readout, which gives the target thermistor resistance

in k Ω while the DISPLAY SET button is depressed. The readout gives the actual thermistor resistance when the button is not pressed.

The current controller supplies an adjustable, low-noise, DC current to power the 808 nm pump laser. Turning up the laser current (top right knob) increases the pump laser current (LED display in mA) and the power in the 532 nm beam, but the relationship is not linear. There is a threshold current of about 130 mA to get any laser power and then the power increases in a roughly quadratic manner with current, but with a small dip around 200-250 mA. The maximum allowable current is around 330 mA and this limit is programmed into the laser current supply and should not be changed.

Even with a steady temperature and current, the 532 nm beam intensity can oscillate at high frequencies with various patterns. Oscillations have been found to be less likely at lower laser temperatures (higher settings on the temperature controller). To see if the laser power is steady, a fraction of the laser power is directed onto a fast photodiode detector (Thorlabs, DET110, see Fig. 1), whose output is monitored on an oscilloscope. If oscillations are present, the laser current or temperature should be adjusted to get rid of them. Laser power fluctuations must be kept small as they will contribute additional fluctuations on top of those from the sample under study.

Using low temperature settings can create a problem with moisture in the air condensing on the laser. This problem shows up as a loss of beam shape and/or a steering of the beam by any water on the laser output surface. It is not usually a problem if the laser is powered because the laser waste heat helps prevent condensation. The problem mostly shows up when the laser has been off for ten minutes or more while temperature controller is left on at

low temperature settings. If the laser current will be off for more than a few minutes, the temperature controller should also be turned off.

Data Acquisition Hardware

Data for this experiment is collected by a multifunction data acquisition (DAQ) module (National Instruments, 6341) and a 640×480 pixel CCD camera (Imaging Source DBK.21AF04.AS). The camera uses a 4.5 mm sensor (SONY, ICX098BQ which has square pixels separated by $5.6 \mu\text{m}$). A color filter array covers the sensor with individual pixels filtered for either red, green, or blue light sensitivity. The DAQ has many inputs and outputs for controlling and monitoring experimental variables. This experiment uses the DAQ timer/counter inputs for monitoring pulses from the PMT and it uses the DAQ 16-bit analog-to-digital converter and amplifier for measuring voltages from the photodiode.

Software

There are three LabVIEW programs for this experiment. The *Monitor* program is used to monitor the PMT count rates and to monitor the laser power as determined from the photodiode. The *FCS* program monitors only the photon counts from the PMT and computes and graphs three quantities: the counts over a user specified time interval as a function of time (essentially a rate meter); a frequency histogram showing the distribution of such counts; and the autocorrelation function averaged over time until stopped by the user. The *FCS Camera* program allows the user to view images and analyze cross sections through them. To take video images or sequences, a fourth program, the NI *Vision* pro-

gram, should be used.

Monitor vi

The monitor program is typically used while adjusting either the laser power or the position of the pinhole P2 (or the the mirror M2) when trying to maximize the overlap of the detection volume with the excitation volume.

The monitor photodiode produces a current I proportional to the laser power P_m incident on its surface. According to the Thorlabs documentation, the sensitivity is about 0.33 amps per watt. The current is converted to a voltage by passing it through a current amplifier (Stanford Research Systems, SR570) characterized by an adjustable transimpedance R_m equal to the output voltage divided by the input current. The SR570 also has filtering circuitry, which should be turned off. The transimpedance $R_m = V/I$ must be specified in ohms in the transimpedance control on the front panel of the *Monitor* program. (R_m is the inverse of the amps/volt sensitivity setting on the SR570.) R_m determines the photodiode current from the measured voltage V . V is monitored by an oscilloscope and simultaneously by an analog to digital converter (ADC channel 0) on the DAQ system. The monitor program averages the ADC voltage over a user-specified averaging time and displays it in the *detector voltage* indicator. This voltage is converted to a current by the user-supplied transimpedance R_m and the current is converted to a incident power by the photodiode sensitivity factor.

The final factor needed is the ratio of the laser power out of the objective to the laser power on the monitor photodiode. This fraction should be determined by the fraction of the 532 nm light transmitted by the dichroic. The specifications for the dichroic, indicate roughly 2% should be transmitted and thus

the factor should be about $98/2$ or around 50. It is determined experimentally by mounting a second photodiode above the objective such that it collects all the laser light out of the objective. The factor so determined then multiplies the monitor power to give the power out of the objective and, except for small losses due to reflections from the coverslip, the power on the sample. Use the default setting for this ratio; redetermining it should only be attempted with the instructor present.

Background light not arising from the laser as well as DC offsets in the amplifiers may also contribute to the ADC readings for the photodiode and so there is a mechanism for subtracting off this component. To use it, simply turn off the laser and click on the *zero detector* button. The laser-off ADC voltage is then read and subtracted from the laser-on voltage before using the conversion factors to obtain the laser power on the sample.

In general, use a transimpedance gain that gives a voltage in the 0.5-5 V range. And be sure to use the lowest possible range on the ADC for measuring that voltage. Allowed ranges are selected in the *Range* control. You must stop and restart the program to change the ADC range.

FCS Camera vi

The instructor will show you how to install the removable mirror so that the magnified image of the sample area will be focused on the camera. The camera has an RGB Bayer filter array over the array of pixels on the CCD sensor so that color information is also available. The red, green and blue pixel images can be overlapped for a color image, or separated for analysis of individual color planes.

The long-pass filter (F1) blocking the 532 nm light can be removed so that one can look at reflections of the laser light from vari-

ous surfaces of the sample, such as the top or bottom of the coverslip to determine the laser spot size w_0 in Eq. 1.

Horizontal or vertical cross sections can be positioned through the areas of the camera image where the fluorescent or reflected spots are located and these one-dimensional cross sections can be saved or analyzed to determine their width and line shape.

The NI Vision program (written by National Instruments) is another program that works with the camera and can be used for additional image analysis tasks or for saving images or video sequences. See the online help for details on this program.

FCS vi

This vi collects data from the PMT module and uses that data to determine and display short term average photon rates, histograms of these rates, and the autocorrelation function and to save the autocorrelation function and/or fit it.

Photons detected by the photomultiplier are converted in the base of its housing unit to 20 ns logic pulses which are routed to a 32-bit counter/timer chip in the DAQ. The DAQ system is programmed to connect a 100 MHz clock signal to the counting input of the counter chip which continually counts these pulses (clock ticks) starting from zero and running up to $2^{32} - 1 = 4.3 \times 10^9$ before overflowing back to zero. Thus, the overflow occurs after about 43 seconds of data collection. The photon pulses from the PMT are routed to the gating input of the counter and on the rising edge of each gate pulse, the counter transfers the current clock tick count to a buffer on the DAQ and then LabVIEW transfers it to main memory for use in the program. The tick count recorded for each photon pulse is thus a *timestamp* (with 10 ns resolution) for

that photon's arrival relative to the start of data acquisition.

The program is set up to accept photons from two separate photomultipliers (data channels A and B) and both can be time-stamped by sending the respective photon pulses to the gates of two different counters. Both counters are programmed to start simultaneously counting the same 100 MHz clock signal. Thus, photons arriving simultaneously in both channels will have the same time-stamp. The data stream consists of continually increasing values of the timestamp t_i^A in clock ticks for the arrival of photons in channel A, and another array of t_j^B giving the time-stamps for the photons in channel B.

The experimental correlation function

The *cross-correlation function* for the photon rates in two PMT detectors is a function of the *delay time* t and is defined by

$$g(t) = \frac{\langle R_A(t')R_B(t'+t) \rangle}{\bar{R}_A\bar{R}_B} \quad (64)$$

where $R_A(t)$ and $R_B(t)$ are the rates of photon detection from each photomultiplier at the time t . As already mentioned in the theory section, the photon rate $R_A(t) = \bar{R}_A + \delta R_A(t)$ can be considered as the sum of its constant average value \bar{R}_A and fluctuations $\delta R_A(t)$ (that will then satisfy $\langle \delta R_A(t) \rangle = 0$). Similarly for $R_B(t)$. With these substitutions, Eq. 64 becomes

$$\begin{aligned} g(t) &= \frac{\langle (\bar{R}_A + \delta R_A(t'))(\bar{R}_B + \delta R_B(t'+t)) \rangle}{\bar{R}_A\bar{R}_B} \\ &= \frac{\langle \bar{R}_A\bar{R}_B + \delta R_A(t')\delta R_B(t'+t) \rangle}{\bar{R}_A\bar{R}_B} \\ &= 1 + \frac{\langle \delta R_A(t')\delta R_B(t'+t) \rangle}{\bar{R}_A\bar{R}_B} \end{aligned} \quad (65)$$

where the cross terms— $\langle \bar{R}_A\delta R_B(t'+t) \rangle = \bar{R}_A \langle \delta R_B(t'+t) \rangle$ and the similar cross term

containing $\delta R_A(t')$ —are both zero (because the fluctuations average to zero) and have been dropped.

The *autocorrelation function* is defined in terms of the rate in a single detector and can be considered as the cross correlation of a signal with itself: $R_B(t) = R_A(t) = R(t) = \bar{R} + \delta R(t)$. With this substitution, Eq. 65 becomes

$$\begin{aligned} g(t) &= 1 + \frac{\langle \delta R(t')\delta R(t'+t) \rangle}{\bar{R}^2} \\ &= 1 + G(t) \end{aligned} \quad (66)$$

where $G(t)$ is the autocorrelation function given in the theory section.

Both $g(t)$ and $G(t)$ are referred to as correlation functions, but experimentally $g(t)$ is more convenient to calculate directly from the photon stream according to the definition: Eq. 64. The averaging indicated by the angle brackets is performed by averaging over long times t' —often several minutes or more. Then either the theoretical $G(t)$ or the experimental $g(t)$ is adjusted according to Eq. 66 to make comparisons or fits to theoretical formulas.

The data acquisition hardware and software are set up to use two photon detectors going to two timer/counters and to compute the cross correlation between their count rates. If only a single PMT detector is used, its pulses must feed both counter/timer gates and would then give that detector's autocorrelation.

Quantum efficiency, dead time, dark counts and afterpulsing

Photon detectors are not ideal.

They have a finite probability of producing an output pulse each time a photon hits their cathode. This probability is the *quantum efficiency* and depends on the photon wavelength. Our detectors have a quantum efficiency around 20% at 500 nm. The quantum

efficiency affects the overall efficiency of the apparatus and little else.

When a pulse is produced by the PMT, the module is “dead” and will not be able to process another incoming photon for a short time thereafter. The dead time for our unit is around 20 ns. The dead time causes an anti-correlation ($G(t) < 0$) for all times below the dead time.

After producing a pulse, and after the dead time, the PMT has an enhanced probability to produce a second pulse. The extra pulse, called an *afterpulse*, arises because a gas molecule in the PMT can become ionized by a cascading electron and then accelerate backward through the electrodes initiating an electron ejection near the cathode or first dynode. This electron then starts another cascade leading to a second pulse. In our apparatus, afterpulsing occurs within a microsecond with a probability of a few percent with virtually no probability after 1 μ s. Since afterpulsing is initiated by a prior pulse, it gives a distinctly shaped, positive contribution to $G(t)$, but only below 1 μ s. There is little effect on the correlation function beyond 1 μ s. You will see the effects of dead time and afterpulsing in your experimental $G(t)$.

Both the dead time and afterpulsing problem are eliminated by splitting the fluorescence into two beams (using a 50-50 beam splitter just after the pinhole) and directing them onto two separate PMTs—one for each beam. The rates from each channel $R_A(t)$ and $R_B(t)$ are then cross-correlated according to Eq. 64 and should give a clean $G(t)$, identical to the autocorrelation for a single detector, but without the artifacts arising from dead time and afterpulsing. The trade-off is a loss by a factor of two in each rate in the calculation.

Thermionic electron emission (emission of thermally energized electrons) from the cath-

ode or first dynode can produce an output pulse called a “dark count.” Room light leaking into the apparatus can also cause counts unrelated to the fluorescence photons. We will refer to all such pulses as “background counts.” We assume the background rate $B(t)$ has a fixed average rate \bar{B} , with natural random fluctuations $\delta B(t) = B(t) - \bar{B}$. The measured photon rate then increases from the theoretical $R(t)$ to the measured rate $R'(t) = R(t) + B(t)$. $B(t)$ is uncorrelated with $R(t)$ (and with itself at all times except $t = 0$).

Exercise 3 Including background counts, the measured autocorrelation function $G'(t)$ for the rate $R'(t)$ then becomes

$$G'(t) = \frac{\langle \delta R'(t') \delta R'(t' + t) \rangle}{\bar{R}'^2} \quad (67)$$

Show that $G'(t)$ would be given in terms of the theoretical $G(t)$ for $R(t)$ according to

$$G'(t) = G(t) \left(1 - \frac{\bar{B}}{\bar{R}'} \right)^2 \quad (68)$$

where $\bar{R}' = \bar{R} + \bar{B}$ is the average rate including the background. Hint: the fact that the background $B(t)$ is uncorrelated with itself means that $\langle \delta B(t') \delta B(t' + t) \rangle = 0$, for all t (except $t = 0$) and that it is uncorrelated with $R(t)$ means $\langle \delta B(t') \delta R(t' + t) \rangle = \langle \delta R(t') \delta B(t' + t) \rangle = 0$ for all t . By what fraction is $G(t)$ attenuated if half the photon rate is due to background?

Correlation algorithm

In order to determine $g(t)$ experimentally, $R(t)$ must first be estimated from the number of counts $N(t)$ occurring over some finite time interval ΔT centered around t , i.e., from $t - \Delta T/2$ to $t + \Delta T/2$. The photon rate over this interval is then given by

$$R(t) = \frac{N(t)}{\Delta T} \quad (69)$$

Measuring over ΔT will average out real fluctuations in the true rate on time scales shorter than ΔT . Consequently, in order to calculate correlations $g(t)$ for a time delay t , the averaging time ΔT must be well less than t .

What happens as ΔT is made smaller? $N(t)$ will be a Poisson random variable. It will come from a distribution with some mean \bar{N} (proportional to ΔT) and a standard deviation $\sigma_N = \sqrt{\bar{N}}$. Assuming ΔT is accurately known, propagation of uncertainty tells us that the relative uncertainty in $R(t)$ is equal to the relative uncertainty in N . (The relative uncertainty in a variable is its standard deviation divided by its mean.) For a Poisson variable, the relative uncertainty $\sigma_N/\bar{N} = 1/\sqrt{\bar{N}}$. Thus, as ΔT is made smaller, the sample values $N(t)$ become smaller and thus have relatively more uncertainty. The calculated $R(t)$ from Eq. 69 will then give a less precise estimate of the true rate over the interval ΔT .

On the other hand, we are not interested in precise values for $R(t)$. We are calculating a correlation function and will be creating products of such rates at different delay times and averaging that product over very long intervals of many seconds. For computing the correlation function, it turns out quite reasonable to use the shortest possible averaging time—one period of the 100 MHz clock or 10 ns! (We will use τ to represent this 10 ns clock period.) This will give terrible estimates for $R(t)$ but perfectly good estimates for $g(t)$ —as long as we average over long times.

First, let's look at the possible measured rates that can be expected if we average over one clock tick. The maximum photon rate will be at least two orders of magnitude lower than the clock frequency. That is, it will be lower than 1 MHz. If the true rate is 1 MHz, the mean number of pulses \bar{N} in any one clock period (10 ns) is $\bar{N} = 0.01$. With this mean, the Poisson probability distribution then suggests

that the probability of no photons in one clock period is $P(0) = (0.01)^0 e^{-0.01}/0! = 0.99$ and 99% of the clock periods will have no pulses in them. The probability of 1 photon in this interval is then $P(1) = (0.01)^1 e^{-0.01}/1! \approx 0.01$ and thus 1% will have one photon. A simple calculation (of $1 - P(0) - P(1)$) indicates a 0.005% chance that 2 or more photons will occur in one clock period. Experimentally, the PMT dead time makes seeing two or more pulses in one clock period impossible. Since our rates are always lower than 1 MHz, we can ignore the small theoretical possibility of such an occurrence without significantly affecting the analysis.

Taking $N = 0$ or $N = 1$ as the only possible values for the total number of photons over the interval τ , the measured rate over any clock period can only be $0/\tau$ if $N = 0$ (no photon during the clock period) or $1/\tau$ if $N = 1$ (one photon during the clock period). Despite the fact that these two measured rates (0 or 100 MHz) will probably never be the true rate, we will see they do give the correct $g(t)$ when applied to that calculation.

Exercise 4 *Show that averaging the two possible rates, 0 and $1/\tau$, at each clock tick (depending on whether or not a photon arrives in that clock tick) gives the correct measured rate $N/\Delta T$ over any interval ΔT during which N pulses arrive.*

An algorithm similar to that of Yang et al. is used to calculate the experimental correlation function from the array of timestamps. It is built around the idea that one uses the two possible measured rates of 0 or $1/\tau$ at each clock tick when computing the correlation function.

To calculate $g(t)$, one must first decide the maximum time delay t^{\max} for which the correlation function needs to be calculated. For the samples studied here, a maximum time around

one second is appropriate. The calculation of $g(t)$ will be performed on a discrete time grid, $t_k = k\tau$, $k = 0, 1, \dots, k^{\max}$, with the spacing between points equal to the clock period τ . The time t^{\max} then determines the grid size $k^{\max} = t^{\max}/\tau$. For $t^{\max} = 1$ s, with $\tau = 10$ ns, the $g(t_k)$ array would contain $k^{\max} = 100$ million grid points.

The quantity inside the time averaging angle brackets in Eq. 64 will be calculated at each clock tick, t_m . Let's call this quantity

$$h_m(t_k) = R_A(t_m)R_B(t_m + t_k) \quad (70)$$

To get $g(t_k)$, one need only average this quantity and then divide by $\bar{R}_A\bar{R}_B$. Each $h_m(t_k)$ will be an array of 100 million values (one for each possible delay time t_k) and it will be evaluated every 10 ns. We have added the subscript m to indicate that that $h_m(t_k)$ is evaluated for one particular clock tick t_m and the average will be computed over $M = T/\tau$ clock ticks where T is some long averaging interval. Thus, the expectation value in Eq. 64 will be approximated by the finite average

$$g(t_k) = \frac{1}{M\bar{R}_A\bar{R}_B} \sum_{m=1}^M h_m(t_k) \quad (71)$$

to get the experimental $g(t)$ on the time grid t_k .

A 100-million point array summed every 10 ns for several seconds would seem to be very computer intensive. As will be seen, there are many less computations than Eq. 71 would suggest. The reason is most of the terms in the sum are zero. If there is no A-photon detected at t_m (no timestamp $t_i^A = t_m$), $R_A(t_m) = 0$ and $h_m(t_k) = 0$ for all k . There is nothing to sum and no calculations are needed until an A-photon arrives during one of the clock ticks. Thus, we only need to calculate $h_m(t_k)$ for those t_m where there is a timestamp in channel A, i.e., for $t_m = t_i^A$. For these clock

ticks, $R_A(t_m) = 1/\tau$, and to get $h_m(t_k)$, this rate must be multiplied by the rate $R_B(t_m + t_k)$ for all t_k up to t^{\max} .

Once again, the rate $R_B(t_m + t_k)$ is zero if there is no B-photon at this clock tick or it is $1/\tau$ if there is a B-photon at this clock tick. Thus, $h_m(t_k)$ is $1/\tau^2$ if there is both an A-photon at $t_i^A = t_m$ and a B-photon at $t_j^B = t_m + t_k$. Otherwise, it is zero.

The algorithm to average $h_m(t_k)$ over long times starts by making a histogram $H(t_k)$ and initializing it with all zeros. Then, the first timestamp in channel A, t_1^A is read and a subarray of timestamps in channel B is created starting with the first one greater than or equal to t_1^A and ending with the last one for which $t_j^B \leq t_1^A + t^{\max}$. This subarray therefore includes all B-timestamps between t_1^A and $t_1^A + t^{\max}$.

The bin at t_k is incremented for each timestamp in channel B at $t_j^B = t_1^A + t_k$. For example, a B-photon at the same timestamp as the one in channel A would cause bin zero to be incremented. A B-photon found one clock tick after t_1^A would cause bin one to be incremented. A B-photon found 1 million clock ticks after t_1^A would cause bin 1 million to be incremented. That is, for each timestamp t_j^B in the B-subarray, the histogram at $t_k = t_j^B - t_1^A$ is incremented.

After incrementing the required bins for every t_j^B in the B-subarray, the timestamp t_2^A for the next photon in channel A is read and the subarray of B timestamps is updated. Timestamps at the beginning are checked and any that are less than the new t_2^A are deleted. If necessary, new B timestamps are read and added to the end of the subarray—again up to and including the last one for which $t_j^B \leq t_2^A + t^{\max}$. The bin-incrementing algorithm is performed again for each timestamp in the B-subarray and the process is repeated for each t_i^A in sequence until $t_i^A > T$, i.e., until acquisi-

tion is stopped at $T = M\tau$.

The program also keeps track of the total number of pulses found in each channel, N_A and N_B , over the averaging time T .

Note that the array of 1's (and 0's) that are added to the histogram for each t_i^A , if divided by τ^2 , is one measured value of $h_m(t_k) = R_A(t_m)R_B(t_m + t_k)$ at the clock tick t_i^A . Recall that $h_m(t_k) = 0$ for every clock tick where there is no timestamp in channel A.

Dividing the histogram by τ^2 thus gives the sum in Eq. 71

$$\sum_{i=1}^M h_m(t_k) = \frac{H(t_k)}{\tau^2} \quad (72)$$

Then, this quantity must be divided by M and by the average rates: $\bar{R}_A = N_A/M\tau$ and $\bar{R}_B = N_B/M\tau$ giving

$$g(t_k) = \frac{MH(t_k)}{N_A N_B} \quad (73)$$

The set of t_k 's for which this calculation is performed would be an equally spaced array with 100 million elements. However, $g(t)$ is typically calculated and displayed on an unequally-spaced grid of less than 1000 elements. This grid is designed to have smaller spacings at shorter t and wider spacings at longer t . This re-binning can be achieved by grouping $g(t_k)$ into sets of adjacent elements—smaller sets of 1 or 2 at the shortest delay times t_k and gradually increasing in proportion to t_k to sets of 1000 or more at longer t_k . The elements within each set are then averaged to determine the $g(t)$ for the t at the middle of the set. The averaging produces a near-logarithmic scaling of the array with points closer together at short times and further apart for longer times. The scaling is reasonable because $g(t)$ around any particular time t is not expected to vary on time scales much shorter than t . The algorithm of Laurence, et al. is actually used to calculate $g(t)$.

It takes less computations than the Yang algorithm by efficiently histogramming data directly into such variably sized bins.

Determining the statistical uncertainty for each point in $g(t)$ and possible correlations between points is quite difficult. It is recommended that you use Poisson weightings (where each point in $H(t_k)$ is assumed to follow a Poisson distribution) and equal weightings (where all points in the fit have the same weight) to see how sensitive fitting parameters are to this choice. Be sure to check residuals to look for systematic deviations between the data and fit.

Procedures

Laser Safety

Note that although this experiment is not dangerous, any eye exposure to the green laser beam would be very dangerous: The beam is very intense, with a power of tens of mW. Serious and permanent eye injury could result if the beam enters your eye. **Proper laser eye safety precautions must be used at any time that the laser is running.**

The apparatus is designed to keep the laser beam enclosed within its intended optical path and away from your eyes. The instrument is safe to use as long as the laser remains enclosed. Therefore, laser safety means that you should not operate the laser when the beam enclosure is open or any portion of the optical pathway has been opened or disassembled. If you open or disassemble any components while the laser is on, you could expose yourself to the beam and suffer a potentially severe injury. Do not attempt to align or adjust any part of the laser optical path.

The only point in the apparatus where the beam leaves its confining path is at the sample slide. In this region the beam is strongly converging/diverging and is not likely to present

a hazard to the user. However you should use common sense and avoid diverting the beam out of this region. Do not place shiny, metallic or reflective objects like mirrors or foil into that region. Do not put your face close to the slide if the laser is on.

General concerns

In addition to laser safety issues, please take care to observe the following precautions

- *Alignment of the optical system:* All optical elements have already been carefully aligned and optimized. The only optical adjustments you will need to make involve manual adjustments to the objective focusing and the positioning of the xy stages holding pinholes P1 and P2. *Please do not attempt to move, disassemble or adjust the laser optics or any of the mirrors, lenses or other optical components.* Any disassembly of the apparatus could also lead to accidental and very dangerous eye exposure to the laser beam.
- *The 100 \times objective:* Please take care that nothing (except immersion oil and lens paper) ever touches the lens of the microscope objective. In focusing or installing the slide, you should not crash or scrape the slide against the lens. When you are finished for the day, please take a single sheet of lens paper and gently wipe the immersion oil from the lens. Do not scrub the lens or use other kinds of wipes: a single wipe with lens paper is fine.

Alignment

Unless there is a change made to the optical layout, you should not need to adjust the two mirrors that steer the laser beam into the spatial filter, the two that steer it into the dichroic

mirror, or the M2 mirror that steers the fluorescence into the pinhole. The instructions given below assume this full alignment as a starting point. If this is the case, a fluorescent signal should be relatively easy to find and only fine adjustments to optimize the signal will be needed. Even then, the instructor will have to demonstrate various alignment steps. If the apparatus is so poorly aligned that a fluorescent signal cannot be found, a full alignment may be needed and, again, the instructor will be needed to demonstrate the required steps.

Diffusion measurements

The autocorrelation function for the diffusion of particles or molecules in water will be used to characterize the measurement volume and to determine the molecular or particle intensity, defined as the number of photons collected per molecule or per particle per unit laser power incident on the sample. This calibration will be performed for both Alexa 532 dye molecules and for small polymer spheres coated with a dye having properties similar to the Alexa dye.

Samples must be freshly diluted from the high concentration stock solutions using proper pipetting techniques. Typical concentrations are 1-10 nM, but one could go a factor of 10-100 in either direction to see how the concentration affects the measurements. Make initial measurements with the 45 nm diameter polystyrene spheres. The stock solution is 5% by weight. Polystyrene density is given as 1.05 g/cc. Make 1500 μl (1.5 cm^3) sphere solution diluted 1:100 to 5×10^{-4} . Then dilute this solution 1:10 to get 5×10^{-5} and then two more times to get concentrations of 5×10^6 and 5×10^{-7} .

Exercise 5 *Determine the 5% stock concentration in units of particles per μm^3 .*

The sample solution can be placed in a homemade microchannel cell. The cell is constructed from two pieces of double-sided tape placed about 5 mm apart near the middle and across the short direction of a regular microscope slide. Use a razor blade to trim away the tape not on the slide. Press a coverslip perpendicular to the slide and centered on the tape channel. Use the back of the razor blade to firmly press the coverslip to the tape and remove as many air bubbles in the adhesive region as possible, but be careful not to break the overhanging cover slip. The 5 mm channel between the tapes is where the sample goes and should be about 50 μm deep.

Put a drop of immersion oil on the coverslip and put this side down on the stage over the objective. Raise the objective to get the immersion oil between it and the coverslip. Use a pipettor and drop about 50 μl of the sample material on top of the coverslip at the channel formed by the tape strips. Watch to ascertain that the solution is forced into the channel by capillary action and then add another 50 μl or so to form small puddles at each end of the channel. The solution evaporates fairly quickly and maintaining a given concentration is thus not easy.

After installing a fluorescent sample in the apparatus, cover the sample area with a sheet of anodize aluminum foil to prevent room light from getting into the objective. Start the *Monitor* program, turn off the room lights, turn on the PMT modules and check the background rate. If it is more than 100 counts/s, find and plug the light leaks.

Always start by adjusting the objective focus and the pinhole P2 to optimize the overlap between the excitation and detection volumes. The instructor will demonstrate how to find a fluorescence signal and make these adjustments.

Raising or lowering the objective changes

the laser focus position relative to the coverslip. The focus should not be too close to the coverslip or the diffusive motion will be modified for particles wandering near the coverslip. The focus should also not be too far from the coverslip because the focusing is not as sharp as it gets further from the coverslip. A reasonable compromise is to raise the objective about 20 μm from the coverslip. The instructor will show you how to adjust the objective focus and how to ascertain the position of the coverslip.

When studying a new molecule, always start with a measurement of the saturation curve—the photon rate vs. the laser power. Both measurements can be made from the *Monitor* program. The laser power is varied using neutral density filters and by changing the laser current. The laser power is measured by the photodiode—properly scaled as described previously. Record and plot the count rate versus laser power. At low laser power, the count rate should be proportional to power. As the power increases, the central part of the laser beam profile will go above the saturation intensity and the count rate will start to fall below the extrapolated low-power linear behavior. Operate at the highest laser power that is still in the the low-power linear regime. Further increasing the laser power will produce smaller increases in the count rate while enhancing deleterious effects due to saturation and photobleaching.

Measure the correlation function for Alexa 532 and for the fluorescent microspheres. Conditions that can be varied include depth of focus above the coverslip, laser power, and concentration. The size of the laser beam coming into the objective and the size of the confocal pinhole P2 can also be changed to see how these parameters affect the results.

Fluorescently-labeled DNA hairpin-loops

DNA hairpin-loops are small single strands of DNA (tens of base pairs) having an affinity for their two ends to bind to one another. The probability for the two ends to come together (making a DNA loop) or break open are different and depend on the size and composition of the loop as well as the temperature and ion concentrations of the buffer solution in which they are measured.

The two ends of the strand are modified so that one end has a fluorophore and the other end has a quencher—a molecule that when brought near the fluorophore prevents it from fluorescing. In the open configuration the DNA fluoresces strongly. In the closed configuration the quencher leads to a much reduced fluorescence. The blinking (fluorescence turning on and off as the DNA opens and closes) appears in the autocorrelation function as a modulation of the normal diffusion term—roughly as given by Eq. 60.

With our current apparatus and DNA stock, the easiest study is to vary the concentrations of Na⁺ ions in the 0.1-1.0 M range by adding that concentration of NaCl into a buffer of 50 μM EDTA and 5mM cacodylic acid, pH 7.0. We have stock solutions of the same DNA strand with and without the quencher.

See the Bonnet, et al. reference for more details.